

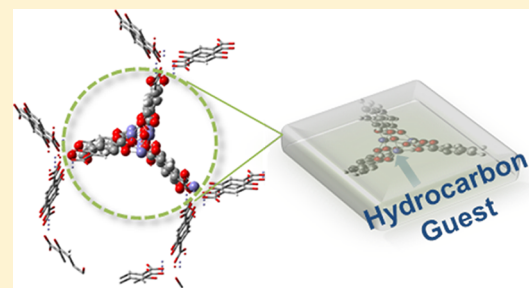
# Adsorption on Fe-MOF-74 for C1–C3 Hydrocarbon Separation

Pragya Verma, Xuefei Xu, and Donald G. Truhlar\*

Department of Chemistry, Chemical Theory Center, and Supercomputing Institute, University of Minnesota, Minneapolis, Minnesota 55455-0431, United States

## Supporting Information

**ABSTRACT:** An increase in demand for energy efficient processes for the separation of a mixture of hydrocarbons drives the need for understanding metal–organic frameworks (MOFs) that can provide better noncryogenic alternatives for the fractionation of hydrocarbon mixtures. Here we study the structure and properties of a metal–organic framework, Fe-MOF-74, and its effectiveness to separate C1–C3 hydrocarbon mixtures. The binding of these hydrocarbons to the open metal sites of Fe-MOF-74 has been investigated using a meta-generalized gradient approximation density functional, M06-L, which has previously been validated for systems containing transition metals. For interpretive purposes, charge model S (CMS) is used to determine the partial atomic charges on the metal cations and the oxygen atoms of the ligands surrounding these metal centers. Our computations show preferential binding to the metal center of Fe-MOF-74 of unsaturated hydrocarbons over saturated ones in agreement with experimental results, and the calculated binding energies are in semiquantitative agreement with experiment. The results are analyzed in terms of various factors contributing to the binding, including structural distortion, electrostatics, damped dispersion, charge transfer, back bonding, and ligand field effects on the d orbitals. The CMS charges are not sensitive to small differences in structure.



## 1. INTRODUCTION

The separation of a mixture of hydrocarbons is a commercially important process that has a wide range of applications in the chemical industry. For example, saturated hydrocarbons find application as fuels, and unsaturated hydrocarbons are widely used in the polymer industry. Current methods of separation, such as cryogenic distillation, which is used to separate a gaseous mixture based on the difference in the boiling points of the constituents, have high-energy costs due to their requirement of low temperatures and high pressure. Metal–organic frameworks (MOFs), which are sponge-like nanoporous materials composed of metal ions and organic linkers, provide a cost-effective alternative to separate C1–C3 hydrocarbons at higher temperatures, dispensing with the need for cryogenic cooling and thus making them promising materials for separation. MOFs exhibit extremely high porosity;<sup>1</sup> they have surface areas surpassing those of zeolites and activated carbons. Their high porosity and the occurrence of open metal sites in some MOFs are pivotal in imparting several crucial functions to these structures such as gas storage,<sup>2</sup> catalysis,<sup>3</sup> and separation of molecular species<sup>4</sup> that can help them act as molecular sieves to fractionate a mixture of light hydrocarbons. The unsaturated coordination sites at the metal center within the bulk of the material allow for the preferential adsorption of one hydrocarbon over the other based on the difference in their electronic properties.

The recently synthesized iron-based MOF, Fe-MOF-74,<sup>5</sup> is a member of the isostructural M-MOF-74 (M = Mg, Mn, Fe, Co, Ni, Cu, and Zn) series (also called the CPO-27 series, where CPO denotes coordination polymer) that has been found to be highly efficient in fractionating C1–C3 hydrocarbon mixtures,

and in particular Fe-MOF-74 is useful for separation of a gaseous mixture of C1–C3 hydrocarbons at a higher temperature than the currently employed cryogenic distillation.<sup>6</sup> The organic fragment of the Fe-MOF-74 is 2,5-dioxido-1,4-benzenedicarboxylate (dobdc<sup>4-</sup>), also called 2,5-dioxidoterephthalate (DOT) in the literature. Fe-MOF-74 has the stoichiometry Fe<sub>2</sub>(dobdc), and it consists of Fe<sup>2+</sup> cations that are linked to each other via the bridging organic linker, dobdc<sup>4-</sup>, to form a framework with hexagonal channels with a diameter of about 1.1 nm.<sup>5</sup> Because of the complexity of the unit cell of Fe-MOF-74 and its large size, it is challenging to model these materials and compute their properties to help in the interpretation of experiments and the design of new MOFs.

Computation has been carried out in the present study by developing a model of Fe-MOF-74 by carving a cluster out of the experimentally reported crystal structure. Herein, we use quantum mechanical density functional methods to study Fe-MOF-74 to understand its high selectivity and its capacity to fractionate mixtures containing methane, ethane, ethylene, acetylene, propane, and propylene (C1–C3 hydrocarbons).

In this work, our specific goal is to understand the structure and binding of C1–C3 hydrocarbon molecules to Fe-MOF-74. The computational study of MOFs is still in its infancy, and a theoretical and computational investigation of the binding of these hydrocarbon molecules adsorbed to the surface of Fe-MOF-74 can be key steps in the future design of new materials.

**Received:** March 24, 2013

**Revised:** May 20, 2013

**Published:** May 22, 2013

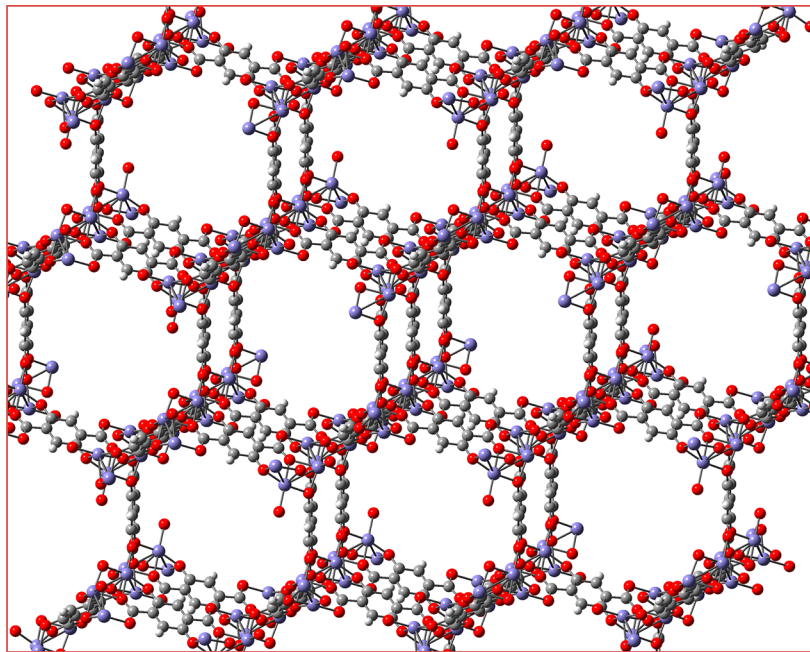


**Figure 1.** Structure of Fe-MOF-74 showing hexagonal channels with the vertices of the channel consisting of three rows of iron centers and the sides consisting of the organic linker, 2,5-diodio-1,4-benzenedicarboxylate ( $\text{dobdc}^{4-}$ ). [Color code: violet = iron, red = oxygen, gray = carbon, white = hydrogen].

## 2. MODEL DEVELOPMENT

To investigate the binding of C1–C3 hydrocarbons to the uncoordinated sites of Fe-MOF-74, two cluster models representative of Fe-MOF-74 have been developed from its crystal structure. The crystal structure is shown in Figure 1.

These models are a compromise in the sense that they are small enough to be studied by reasonably accurate density functional calculations but large enough to include the main physical features controlling the binding. In particular, three-iron and five-iron models with increasing levels of resemblance to its crystal structure were carved out of the crystal structure<sup>5</sup> of Fe-MOF-74. These structures have 88 and 106 atoms, respectively. These models were obtained by considering one of the iron ions as the central iron ion in the crystal structure of Fe-MOF-74 and by drawing an 8 Å radius around this central iron ion in a manner similar to what is done for QM/MM partitioning (Figure 2). All atoms beyond 8 Å from the central atom were truncated, and some atoms within 8 Å of the central atom were also removed to obtain cluster models consisting of three and five iron ions.

**Three-Iron Model.** The three iron ions of the three-iron model have their open coordinated sites pointing toward three surrounding hexagonal channels in which a guest molecule can interact with an iron (Figure 3). This model has six organic ligands, with a pair of ligands in each of the three channel walls that intersect at the vertex (also called pillar or *c* axis) that contains the iron centers. Every iron ion formally has two units of positive charge, and hence three iron ions in the model make a total of six units of positive charge that need to be balanced by negative charges on the ligands to make the structure neutral. The initially truncated structure had an excess of negative charge due to the presence of negatively charged functional groups, carboxylate ( $\text{COO}^-$ ) and oxido ( $\text{O}^-$ ), on the  $\text{dobdc}^{4-}$  linker because the linker functionalities at the edges of the simply truncated cluster would be uncoordinated to any of the iron centers. The simply truncated structure was neutralized by a combination of two procedures: (1) removing the negatively

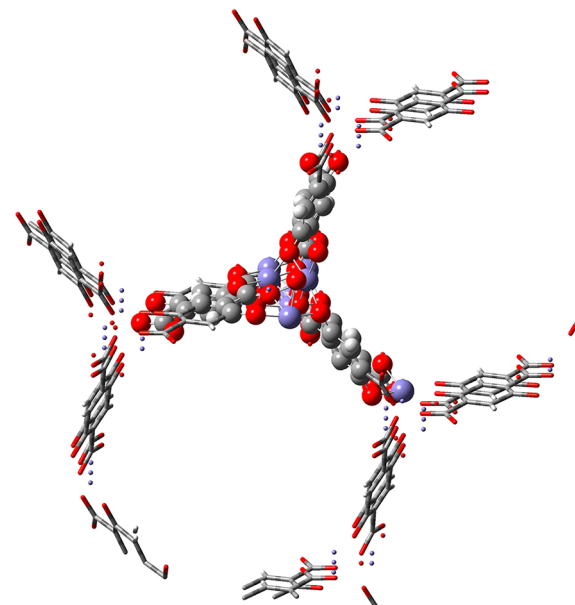


**Figure 2.** Fragment of Fe-MOF-74 showing one of the vertices formed at the junction of three hexagonal channels. Iron ions are arranged in a helical column along each vertex. The atoms, that are within 8 Å of one of the iron ions, are shown as a ball-and-stick model, and atoms beyond 8 Å are rendered as wireframe; this fragment of the MOF includes eight iron ions, 41 carbons, 30 oxygens, and 11 hydrogens. [Color code: violet = iron, red = oxygen, gray = carbon, white = hydrogen].

charged carboxylate and oxido groups that were away from the central pillar of the iron ions in the organic linker,  $\text{dobdc}^{4-}$ , and capping the resultant structure using hydrogen atoms and (2) neutralizing three of the carboxylate groups participating in the coordination environment of iron ions along the pillar by adding hydrogen atoms. The resulting neutral structure has 88 atoms with the central iron ion having a tetrahedral pyramidal

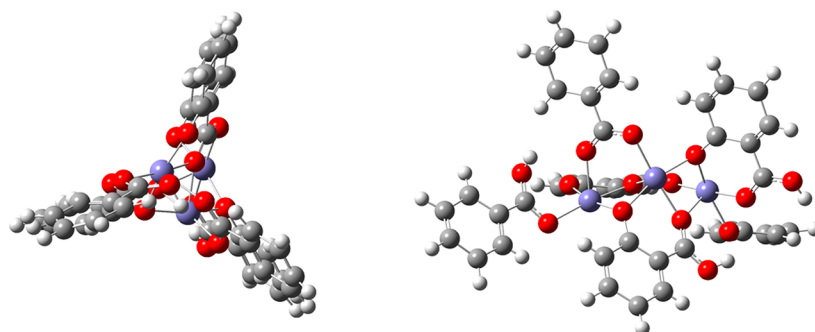


**Figure 3.** Three-iron model of Fe-MOF-74 carved out of the crystal structure viewed along the *c* axis (left) and perpendicular to the *c* axis (right). [Color code: violet = iron, red = oxygen, gray = carbon, white = hydrogen].

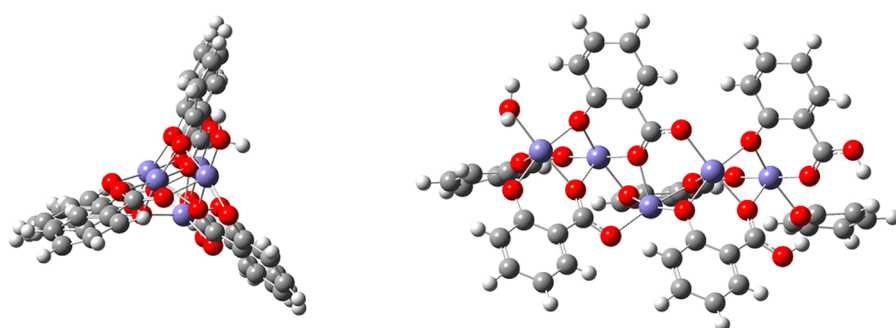
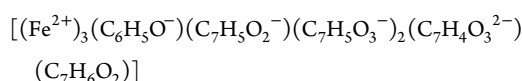
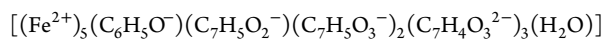


**Figure 4.** Five-iron model of Fe-MOF-74 carved out of the crystal structure viewed along the *c* axis (left) and perpendicular to the *c* axis (right). [Color code: violet = iron, red = oxygen, gray = carbon, white = hydrogen].

coordination of five oxygen ligands around it in precisely the same manner as in the crystal structure. Also, the peripheral iron ions are pentacoordinate with oxygen ligands again in a tetragonal pyramid around it. They deviate slightly from the crystal structure of Fe-MOF-74 because of the presence of oxygen ligands directly coordinated to these iron ions having hydrogen atoms that are not present in the crystal structure of Fe-MOF-74. This three-iron model has been created by taking care that the environment around the central iron ion is preserved, while that around the two terminal iron ions is allowed to deviate from the actual structure of the MOF to maintain neutrality of the structure. This 88-atom model has the stoichiometry



**Five-Iron Model.** A five-iron model has also been created. It has 106 atoms and is shown in Figure 4. In this model two of the iron ions (the central iron and one which is 3 Å to the left of it) have coordination environments that precisely mimic the immediate environment of iron ions in the crystal structure. This is unlike the three-iron model where only the central iron ion fully preserves the nearby coordination environment. This five-iron model has one water molecule, five Fe ions, and seven organic linkers. The water molecule is added to satisfy the distorted tetragonal pyramidal coordination (penta-coordination) environment around one of the terminal Fe ions. Five iron ions contribute to a total of ten units of positive charge, which is balanced by negative charges on the organic linkers to obtain a neutral structure. This 106-atom model has the stoichiometry



### 3. THEORETICAL AND COMPUTATIONAL DETAILS

The accuracy and computational economy provided by density functional methods make them a natural choice for our calculations on large MOF clusters. The exact exchange–correlation functional is unknown, and practical density functional calculations require using an approximate functional. We employ a meta-generalized gradient approximation to the exchange–correlation functional, M06-L,<sup>7</sup> to study the structure and properties of Fe-MOF-74 and the binding of C1–C3 hydrocarbons to it. M06-L is extensively validated for studying the thermochemistry of transition metals, and because it is a local density functional with no Hartree–Fock exchange, it is affordable for very large systems.<sup>8</sup> The cost of the calculations is further reduced by the use of a density-fitting method with the fitting basis generated automatically by the Gaussian 09 program.<sup>9</sup> The basis set used for our calculations is the def2-TZVP basis set (TZVP = valence triple- $\zeta$  polarized) which has been developed by the Ahlrichs group.<sup>10</sup>

We investigate the binding of C1–C3 hydrocarbons to the central iron ion of the 88-atom model. We used the 106-atom model only for ethane and ethylene because of the higher computational cost involved in the larger model. We restrict each iron(II) site to be in a quintet high-spin state; this choice has been considered for our calculations based on reports in the literature of transition metals in M-MOF-74 being in a high spin state.<sup>6,11</sup> In addition, one expects a high spin state because oxygen ligands are among the weak ligands in the spectrochemical series.<sup>12</sup>

The 88-atom model has three iron ions, each in a high-spin state ( $|M_S| = 2$ ). We assign an  $M_S$  value of either 2 or -2 to each of the three iron centers. Four possibilities for assigning the  $M_S$  values to these iron centers have been considered. If a local spin state of  $M_S = 2$  is assigned to all three iron centers, it is called the

222 state. An assignment of a local spin state of  $M_S = 2$  on the left and the central iron centers and  $M_S = -2$  on the right iron center gives rise to the 22 $\bar{2}$  spin state resulting in the overall spin state of the model being  $M_S = 2$ . When only the central iron is assigned a local spin state of  $M_S = -2$  while the peripheral iron centers have a local spin state of 2, it gives rise to the 2 $\bar{2}2$  state with (again)  $M_S = 2$ . In the final case, the central and the right iron centers have a local spin state of  $M_S = 2$ , and the left iron center has an  $M_S = -2$  spin state leading to the  $\bar{2}22$  state. Binding energies and enthalpies have been computed for all four spin states.

For the larger 106-atom model with five iron ions, in the present work, we only consider one high-spin state 22222, which assigns each of the five iron centers a local spin state of  $M_S = 2$ . The reason that only the high-spin state has been considered is our observation that the 88-atom model does not show a significant variation in binding enthalpies for all the four spin states considered here (this is documented in the Supporting Information).

For some calculations, we optimized the coordinates of one or more of the atoms in the cluster, while holding the other atoms at their positions in the crystal structure; we denote the number of atoms whose coordinates are optimized as  $n_{\text{opt}}$ . The rationale behind optimizing atoms within the cluster is to observe the effect on the binding energy of relaxing the geometry. As the guest molecule approaches the central metal ion of the bare cluster, it is important to optimize the position of the metal atom in the binding site to accommodate the new ligand, and it might be important to optimize the positions of additional atoms as well. However, if too many atoms in the cluster are optimized, there is a danger that the orientation of the ligands will no longer match that required by the periodic structure of the framework. So the best compromise might be to optimize only the position of the central metal atom, but since the best compromise is not known, we present results for three extents of optimization (with  $n_{\text{opt}} = 0, 1$ , and 12). The resulting structures were confirmed to be minima in the optimized degrees of freedom by doing partial frequency calculations on these structures. The absence of imaginary frequencies characterized the stationary points as minima.

The binding enthalpies of the guest molecule bound to the MOF cluster were calculated at temperatures ( $T$ ) of 298.15 and 318 K, where the latter temperature was chosen so that we could compare our computed values with the experimental data<sup>6</sup> available on the adsorption enthalpies at 318 K. In the case where no atom of the cluster is optimized and only the guest molecule coordinates are optimized for both the isolated guest and the adsorbed guest structures, the formula employed to compute the binding enthalpy of a guest molecule to the central metal ion of the cluster is

$$\Delta H_T = \Delta E_{\text{BO}} + E_{\text{vib}}(\text{guest}) + E_{\text{trans}}(\text{guest}) + E_{\text{rot}}(\text{guest}) \\ - E_{\text{vib}}(\text{cluster-guest}) + RT \quad (1)$$

where  $\Delta E_{\text{BO}}$  is the change in Born–Oppenheimer energy (electronic energy plus nuclear repulsion) upon binding;  $\Delta E_{\text{BO}}$  is given by

$$\Delta E_{\text{BO}} = E_{\text{BO}}(\text{cluster}) + E_{\text{BO}}(\text{guest}) - E_{\text{BO}}(\text{cluster-guest}) \quad (2)$$

$E_{\text{vib}}(\text{cluster-guest})$  is the vibrational energy of the  $3n_{\text{opt}}$  frequencies (here  $n_{\text{opt}} = n_g$ , where  $n_g$  is the number of atoms of the guest) of the cluster–guest complex; and  $E_{\text{vib}}(\text{guest})$  is the vibrational energy of the  $3n_{\text{opt}} - 5$  frequencies of isolated

acetylene or  $3n_{\text{opt}} - 6$  frequencies of the rest of the five isolated guest molecules.  $E_{\text{trans}}$  and  $E_{\text{rot}}$  are, respectively, translational and rotational energies, which are included only for the isolated guest because the crystal has neither translational nor rotational degrees of freedom; the final term of eq 1 is the pressure–volume contribution for the loss of one mole of ideal gas; and  $R$  is the gas constant.

Similarly, when  $n_{\text{opt,c}}$  atoms of the cluster are allowed to relax along with  $n_g$  atoms of the guest molecule, the formula used to calculate the binding enthalpy of a guest molecule to the central metal ion of the cluster is

$$\Delta H_T = \Delta E_{\text{BO}} + E_{\text{vib}}(\text{cluster}) + E_{\text{vib}}(\text{guest}) + E_{\text{trans}}(\text{guest}) \\ + E_{\text{rot}}(\text{guest}) - E_{\text{vib}}(\text{cluster-guest}) + RT \quad (3)$$

where  $E_{\text{vib}}(\text{cluster-guest})$  is the contribution to thermal energy arising from  $3(n_g + n_{\text{opt,c}})$  vibrational modes of relaxed atoms in the cluster–guest complex;  $E_{\text{vib}}(\text{cluster})$  is based on  $3n_{\text{opt,c}}$  vibrational modes; and the other terms are the same as in eq 1.

The partial atomic charges on both the iron centers and the dobdc<sup>4-</sup> organic linkers were calculated using the CMS-PAC package<sup>13</sup> that utilizes Hirshfeld atomic charges<sup>14</sup> calculated by Gaussian 09 to obtain partial atomic charges by Charge Model 5<sup>15</sup> (CMS) by mapping.

All density functional theory calculations were performed using the Gaussian09 suite of quantum chemical programs. The ultrafine (99 radial nodes and 590 angular nodes) grid (or a grid with 99 radial nodes and 974 angular nodes) is used for density functional integrations, and the symmetry of the Kohn–Sham Slater determinant is allowed to break and converge to the broken symmetry solution using the Stable = Opt keyword of Gaussian 09.

## 4. RESULTS AND DISCUSSION

**Structures of Unoptimized and Optimized Cluster Models.** The crystal structure of Fe-MOF-74 has repeating units of iron ions, each surrounded by five oxygen ligands in a tetragonal pyramidal coordination shell (Figure 5). The

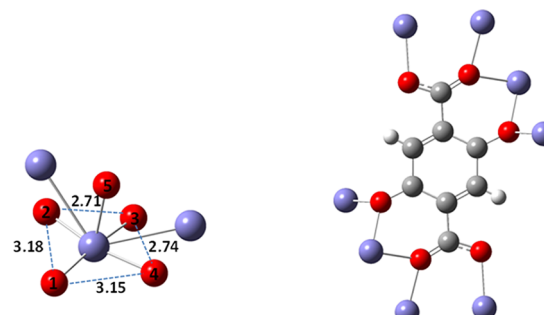


**Figure 5.** Environment around the iron center and the organic linker, 2,5-dioxido-1,4-benzenedicarboxylate (dobdc<sup>4-</sup>). [Color code: violet = iron, red = oxygen, gray = carbon, white = hydrogen].

arrangement of the five oxygen atoms around an iron center deviates from a perfect square pyramidal arrangement. The distances of the iron center from the five oxygen atoms in its first coordination sphere that are labeled as O1, O2, O3, O4, and O5 in Figure 5 are 2.17, 1.99, 2.11, 2.07, and 2.13 Å, respectively. All five of these Fe–O distances in the first coordination sphere of an iron center are longer than the sum of the covalent radii of Fe and O, which is<sup>16</sup>  $1.24 + 0.64 = 1.88$  Å. Each iron center also has two

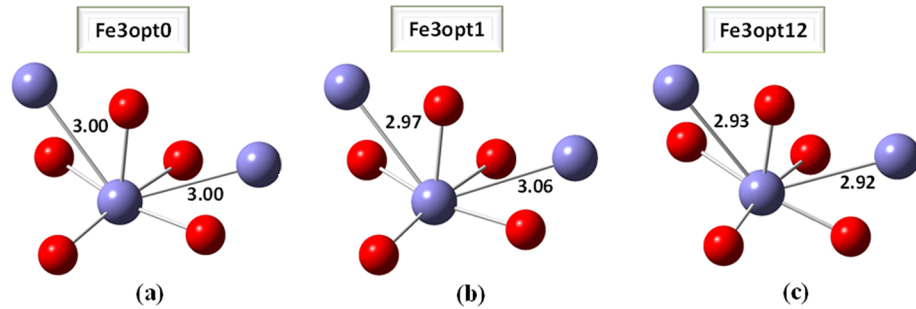


**Figure 6.** (a) Fe3opt0: no atom is optimized. (b) Fe3opt1: only the central iron ion is optimized. (c) Fe3opt12: the central iron ion and 11 atoms in the first coordination shell of the iron ion are optimized. Some distances are given in Å. [Color code: violet = iron, red = oxygen].

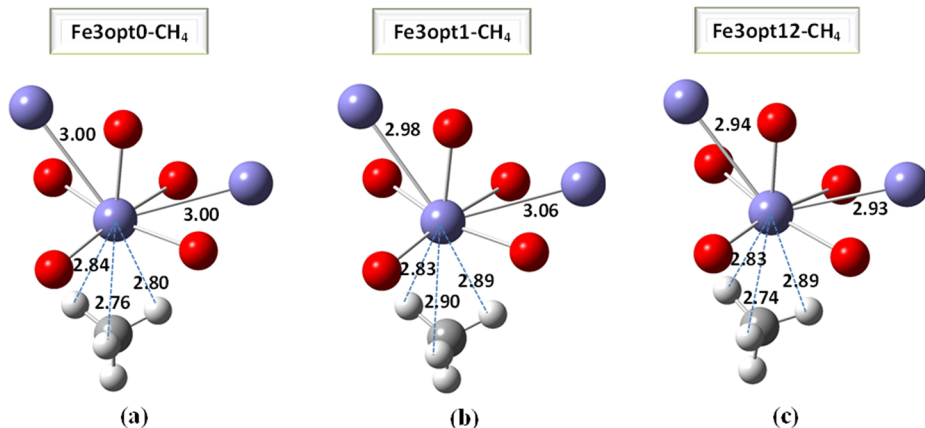


**Figure 7.** (a) Fe3opt0-CH<sub>4</sub>: only methane is optimized, and no atom of the cluster is optimized. (b) Fe3opt1-CH<sub>4</sub>: only the central iron ion of the cluster and methane bound to it are optimized. (c) Fe3opt12-CH<sub>4</sub>: the central iron, 11 atoms in the first coordination shell of the central iron ion, and methane bound to the central iron ion are optimized. Some distances are given in Å. [Color code: violet = iron, red = oxygen, gray = carbon, white = hydrogen].

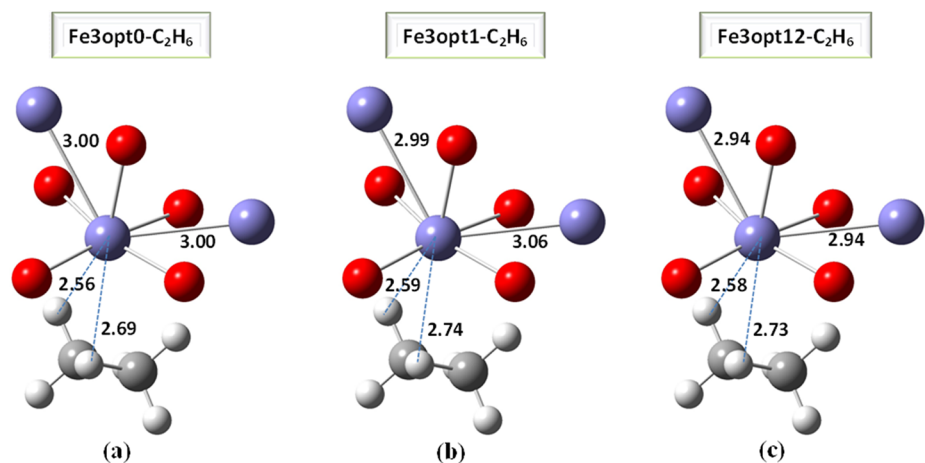


**Figure 8.** (a) Fe3opt0-C<sub>2</sub>H<sub>6</sub>: only ethane is optimized, and no atom of the cluster is optimized. (b) Fe3opt1-C<sub>2</sub>H<sub>6</sub>: only the central iron ion of the cluster and ethane bound to it are optimized. (c) Fe3opt12-C<sub>2</sub>H<sub>6</sub>: the central iron, 11 atoms in the first coordination shell of the central iron ion, and ethane bound to the central iron ion are optimized. Some distances are given in Å. [Color code: violet = iron, red = oxygen, gray = carbon, white = hydrogen].

iron ions that are each 3 Å away; these may be considered to be part of a second coordination sphere. Four of the oxygens are almost planar, as shown in Figure 5. These four oxygen atoms are arranged in the shape of a kite (not a square).

The dobdc<sup>4-</sup> organic fragment of the Fe-MOF-74 coordinates to eight metal centers, four on each of its sides (Figure 5). The coordination on both sides of the linker is precisely the same. Every inorganic/organic fragment that comprises Fe-MOF-74 is

equivalent, with every iron ion in the Fe-MOF-74 having an identical environment around it and every dobdc<sup>4-</sup> surrounded by metal centers in precisely the same fashion as shown in Figure 5. The open sites of iron ions, also called activated sites (because they are opened up by evaporating solvent), open into three hexagonal channels where a hydrocarbon (guest) molecule may bind (adsorb).

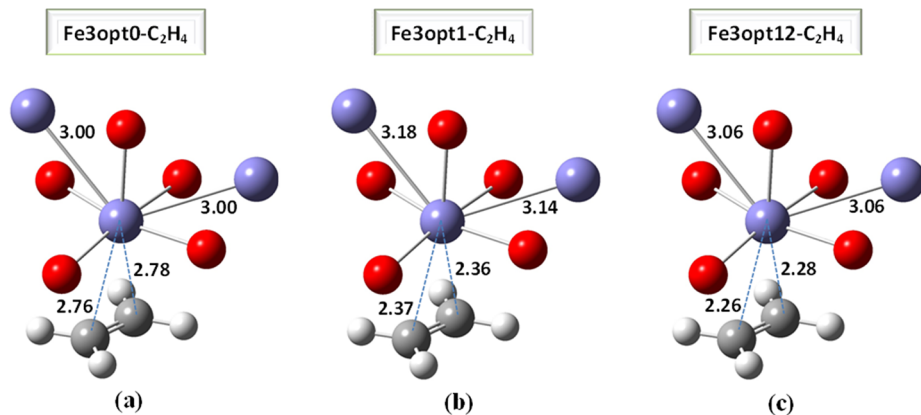


**Figure 9.** (a) Fe3opt0–C<sub>2</sub>H<sub>4</sub>: only ethylene is optimized, and no atom of the cluster is optimized. (b) Fe3opt1–C<sub>2</sub>H<sub>4</sub>: only the central iron ion of the cluster and ethylene bound to it are optimized. (c) Fe3opt12–C<sub>2</sub>H<sub>4</sub>: the central iron, 11 atoms in the first coordination shell of the central iron ion, and ethylene bound to the central iron ion are optimized. Some distances are given in Å. [Color code: violet = iron, red = oxygen, gray = carbon, white = hydrogen].

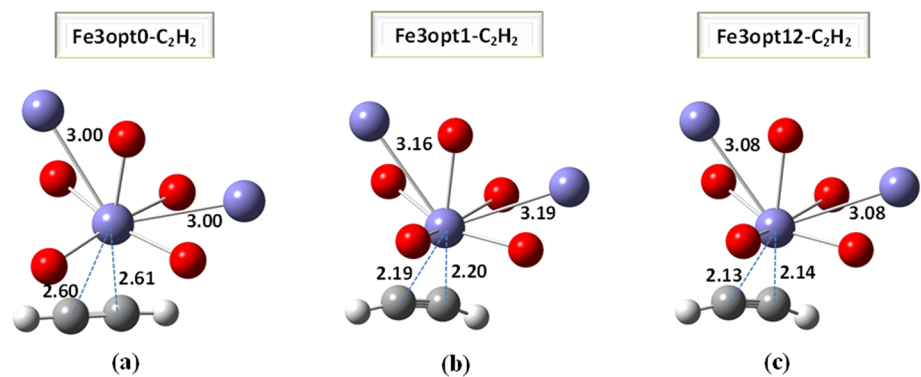


**Figure 10.** (a) Fe3opt0–C<sub>2</sub>H<sub>2</sub>: only acetylene is optimized, and no atom of the cluster is optimized. (b) Fe3opt1–C<sub>2</sub>H<sub>2</sub>: only the central iron ion of the cluster and acetylene bound to it are optimized. (c) Fe3opt12–C<sub>2</sub>H<sub>2</sub>: the central iron, 11 atoms in the first coordination shell of the central iron ion, and acetylene bound to the central iron ion are optimized. Some distances are given in Å. [Color code: violet = iron, red = oxygen, gray = carbon, white = hydrogen].

We introduce the following notations to describe each of the optimized and unoptimized structures (all unoptimized coordinates are taken from the experimental crystal structure). Fe3opt0 stands for the 88-atom cluster where no atom is optimized (all atoms are frozen). In Fe3opt1, only one atom, which is the central iron ion, is optimized, and the remaining 87 atoms are frozen during geometry optimization. In Fe3opt12, 12 atoms are optimized; these include the central iron ion and 11 atoms of the groups in the first coordination sphere (three carboxylates and two oxidos in the first coordination sphere of the central iron), and the remaining 76 atoms are kept frozen during geometry optimization. When any of the above structures is optimized along with the guest molecule (which is a C<sub>1</sub>–C<sub>3</sub> hydrocarbon), whose coordinates are always optimized, the structures are called Fe3opt0–guest, Fe3opt1–guest, and Fe3opt12–guest, respectively. The structures of both the bare MOF and the MOF bound to a hydrocarbon molecule for the lowest energy spin state of the three iron centers, which is the 222 state (the spin structure notation is described in more detail in Section 3), are shown in Figures 6–12.

In Figure 6, it can be observed that, as the number of optimized atoms in the cluster increases from 0 to 1 (Fe3opt0 and Fe3opt1 systems, respectively), the central iron ion moves away from its position asymmetrically with respect to the neighboring iron ions as shown by a difference in bond distances of the central iron ion

from the peripheral iron ions in Figure 6b. This phenomenon can also be observed in the presence of a guest molecule (see Figures 7b–12b). For the Fe3opt12 systems, the central iron ion moves more or less symmetrically with respect to the peripheral iron ions. The maximum difference in the bond distances for Fe3opt12 systems is 0.02 Å, which is observed for Fe3opt12–C<sub>3</sub>H<sub>8</sub> (Figure 11c).

In Figures 7, 8, and 11, it can be observed that the three saturated hydrocarbons (methane, ethane, and propane) are bound to the central iron ion through their C–H bonds. Moreover, the distances of the central iron ion from the nearest hydrogen atoms are unequal. This result is consistent for all three levels of optimization. The C–H bonds of methane, ethane, and propane directed toward the iron center become slightly elongated compared to the length optimized for the free hydrocarbon. This elongation is ~0.003 Å for the three C–H bonds of methane. For ethane and propane we center attention on the two hydrogens closest to Fe. The C–H bond lengths of these hydrogens elongate by ~0.003–0.004 Å in ethane and by 0.003–0.005 Å in propane.

The unsaturated hydrocarbons are bound to the central iron ion by their C–C double or triple bonds rather than through C–H bonds. For acetylene and ethylene, the distances of the central iron ion from the two carbon atoms are almost equal (Figures 9 and 10). The Fe–C distances for ethylene, acetylene, and

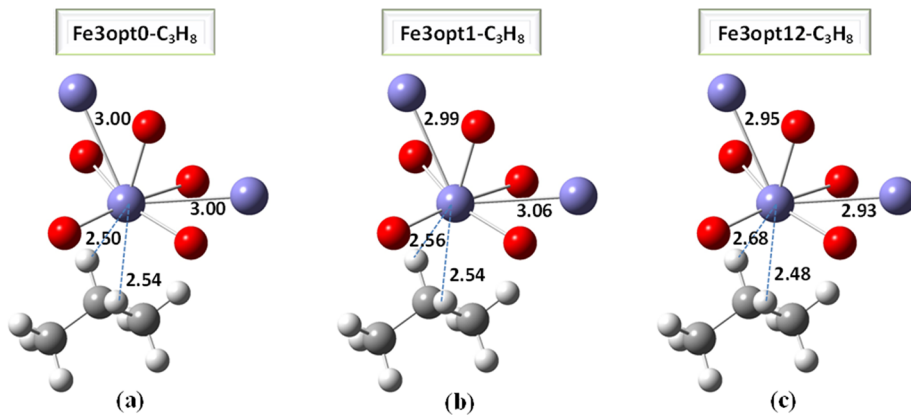


**Figure 11.** (a) Fe3opt0–C<sub>3</sub>H<sub>8</sub>: only propane is optimized, and no atom of the cluster is optimized. (b) Fe3opt1–C<sub>3</sub>H<sub>8</sub>: only the central iron ion of the cluster and propane bound to it are optimized. (c) Fe3opt12–C<sub>3</sub>H<sub>8</sub>: the central iron, 11 atoms in the first coordination shell of the central iron ion, and propane bound to the central iron ion are optimized. Some distances are given in Å. [Color code: violet = iron, red = oxygen, gray = carbon, white = hydrogen].

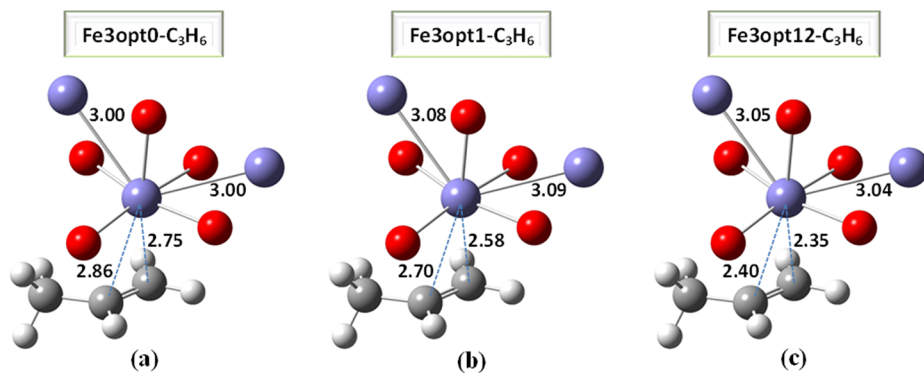


**Figure 12.** (a) Fe3opt0–C<sub>3</sub>H<sub>6</sub>: only propylene is optimized, and no atom of the cluster is optimized. (b) Fe3opt1–C<sub>3</sub>H<sub>6</sub>: only the central iron ion of the cluster and propylene bound to it are optimized. (c) Fe3opt12–C<sub>3</sub>H<sub>6</sub>: the central iron, 11 atoms in the first coordination shell of the central iron ion, and propylene bound to the central iron ion are optimized. Some distances are given in Å. [Color code: violet = iron, red = oxygen, gray = carbon, white = hydrogen].

propylene are intermediate between standard single bond lengths<sup>16</sup> ( $1.24 + 0.75 = 1.99$  Å) and van der Waals distances<sup>16</sup> ( $2.04 + 1.70 = 3.74$  Å), and this situation is also observed experimentally.<sup>6</sup> The Fe–C distances of propylene in the Fe3opt1 model agree with the experimentally reported results better than do the Fe–C distances of ethylene and acetylene. A decrease in the Fe–C distance is observed upon increasing the number of atoms being optimized within the cluster (Figures 9c, 10c, and 12c). This is because relaxation of more atoms within the cluster causes stronger binding and hence brings the unsaturated hydrocarbon closer to the metal ion. The lengths of the C–C multiple bonds have been found to increase upon binding to Fe and also upon increasing the extent of optimization from Fe3opt0 to Fe3opt12. For example, the C–C double bond in ethylene increases from 1.32 Å when free to 1.33 Å for Fe3opt0–C<sub>2</sub>H<sub>4</sub>, to 1.35 Å for Fe3opt1–C<sub>2</sub>H<sub>4</sub>, and to 1.36 Å for Fe3opt12–C<sub>2</sub>H<sub>4</sub>. The C–C triple bond in acetylene increases from 1.20 Å in free acetylene and Fe3opt0–C<sub>2</sub>H<sub>2</sub> to 1.22 Å in Fe3opt1–C<sub>2</sub>H<sub>2</sub>, and to 1.23 Å in Fe3opt12–C<sub>2</sub>H<sub>2</sub>. In the case of propylene, the C–C double bond increases from 1.32 Å when free to 1.33 Å for Fe3opt0–C<sub>3</sub>H<sub>6</sub>, to 1.34 Å for Fe3opt1–C<sub>3</sub>H<sub>6</sub>, and to 1.35 Å for Fe3opt12–C<sub>3</sub>H<sub>6</sub>. Along with the increasing number of optimized atoms, the stronger electron back-donation from the 3d orbital of the central metal ion to the C–C  $\pi$  antibonding orbital of unsaturated guest molecules is observed as

discussed in later NBO analysis section. This is why there is an increase in C–C multiple bond length with increasing level of optimization.

The experimental Fe–H distances are 2.6 Å for two hydrogen atoms of ethane directed toward iron and 2.9 and 2.2 Å for the two hydrogen atoms in propane directed toward the iron center.<sup>6</sup> Comparison to Figures 8 and 11 shows good agreement with experimental distances for all three levels of optimization for ethane, but theory leads to Fe–H bonds for propane somewhere in between 2.9 and 2.2 Å. The experimental Fe–C distances are, respectively, 2.4, 2.5, and 2.6 Å in ethylene, acetylene, and propylene. Comparison to Figures 9, 10, and 12 shows the best agreement with opt1 structures in two cases and with opt0 in the other; in contrast, the opt12 structures are too tightly bound by 0.1, 0.4, and 0.2 Å, respectively.

**Binding Enthalpies.** Four spin states of the 88-atom cluster model were studied by considering each of the possible combinations of local quintet states on each of the three iron ions. Enthalpies for binding of both saturated and unsaturated hydrocarbons at the central iron ion were computed. We have computed only the binding enthalpies at both 298.15 and 318 K and not the Gibbs free energies and entropies because the experimental data<sup>6</sup> are available only for enthalpies of adsorption. Furthermore, free energy and entropy calculations involve additional uncertainties that are beyond the scope of the present

article. Hence, we confine ourselves to discussions of binding energies and binding enthalpies.

Table 1 gives results only for the 222 spin state because it is the lowest-energy spin state of the MOF; results for other spin states

**Table 1. Binding Energies and Enthalpies (kcal/mol) Calculated for the Adsorption of a Guest Molecule at the Central Iron Ion of the 88-Atom Model for the 222 Spin State**

guest	calculated			experimental $\Delta H_{318}$
	$\Delta E$	$\Delta H_{298.15}$	$\Delta H_{318}$	
(Fe3opt0–guest)				
methane	7.8	6.8	6.7	4.8
ethane	8.8	7.6	7.5	6.0
ethylene	12.3	11.0	10.9	10.8
acetylene	12.3	11.8	11.8	11.2
propane	9.9	8.6	8.6	7.9
propylene	14.3	13.0	13.0	10.5
(Fe3opt1–guest)				
methane	6.7	5.6	5.6	4.8
ethane	8.3	7.1	7.0	6.0
ethylene	11.9	10.8	10.7	10.8
acetylene	12.7	12.4	12.4	11.2
propane	9.8	8.6	8.5	7.9
propylene	14.2	13.0	12.9	10.5
(Fe3opt12–guest)				
methane	6.6	5.5	5.4	4.8
ethane	8.5	7.3	7.3	6.0
ethylene	15.1	14.0	14.0	10.8
acetylene	14.5	14.3	14.2	11.2
propane	9.0	7.6	7.6	7.9
propylene	16.5	15.4	15.3	10.5

are given in Tables S1, S2, and S3 of the Supporting Information. At 318 K, the binding enthalpies for other spin states always agree with those for the 222 spin state within 0.1 kcal/mol for ethane, 0.3 kcal/mol for propylene, and 0.4 kcal/mol for methane, but the deviations are much larger—up to 1.2 kcal/mol—for ethane and ethylene. Here we discuss only the 222 spin state.

It can be seen from Table 1 that the unsaturated hydrocarbons bind more strongly to the central metal ion than do the saturated ones. Since different hydrocarbons bind to the metal centers with different strengths, a mixture of such hydrocarbons when passed through Fe-MOF-74 can be separated based on their differential adsorption within the pore of the MOF.<sup>6</sup> Table 1 also indicates that binding through the C–C double or triple bond to the iron center is stronger than that occurring through the C–H bond. Moreover, the values obtained by the M06-L/def2-TZVP method agree well with the experimental values<sup>6</sup> for the opt0 and opt1 structures, each having a mean absolute deviation (MAD) from experiment of only 1.0 kcal/mol (average over six cases). Comparison of the binding enthalpies for methane in Table 1 indicates that as more atoms of the 88-atom cluster are optimized the values get closer to the experimental value of 4.8 kcal/mol. This can also be seen for propane (which is interesting in light of the discrepancy with experiment for Fe–H distances), but for ethane, there is no significant change in binding enthalpies from Fe3opt1 to Fe3opt12. For the unsaturated hydrocarbons ethylene, acetylene, and propylene, the binding is strongest for the Fe3opt12 case because the unsaturated carbon atoms get closer to the central iron ion as can be seen in Figures 9, 10, and 12. However, the Fe3opt12 results of all three unsaturated hydrocarbons overestimate the binding enthalpies

by 3–5 kcal/mol compared to the experimental data, leading to an increased MAD of 2.2 kcal/mol for the average over six cases. This overbinding of the unsaturated adsorbates is consistent with the too short Fe–C bond distances in the opt12 structures for these cases, which was already discussed.

Table 2 compares the binding energies of ethane and ethylene in the 88-atom ( $\text{Fe}_3$  system) and 106-atom ( $\text{Fe}_5$  system) models.

**Table 2. Comparison of Binding Energies (kcal/mol) of  $\text{Fe}_3$  (222 Spin State) and  $\text{Fe}_5$  (22222 Spin State) Model Systems Bound to Ethane and Ethylene<sup>a</sup>**

$\text{Fe}_5$ systems	$\Delta E$	$\text{Fe}_3$ systems	$\Delta E$
Fe5opt0–ethane	10.2	Fe3opt0–ethane	8.8
Fe5opt1–ethane	9.6	Fe3opt1–ethane	8.3
Fe5opt0–ethylene	13.0	Fe3opt0–ethylene	12.3
Fe5opt1–ethylene	15.5	Fe3opt1–ethylene	11.9

<sup>a</sup>All calculations were done by M06-L/def2-TZVP.

The difference averages 1.8 kcal/mol, which is surprisingly large. The structures for Fe5opt1 complexes are shown in Figure 13; comparison to Figures 8(b) and 9(b) shows very good agreement.

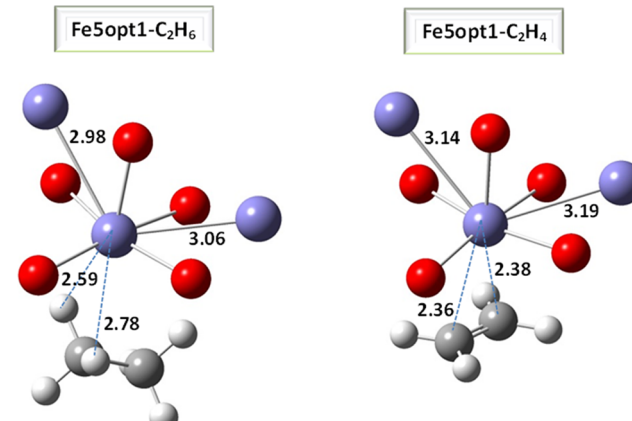


**Figure 13.** (left)  $\text{Fe5opt1}-\text{C}_2\text{H}_6$  and (right)  $\text{Fe5opt1}-\text{C}_2\text{H}_4$ . Some distances are given in Å. [Color code: violet = iron, red = oxygen, gray = carbon, white = hydrogen].

**Dispersion Energy.** There is considerable current interest in the role of dispersion-like interactions in the chemistry of materials. The partition of molecular interactions into dispersion, induction (polarization), and permanent-moment electrostatics is unique in the long-range, zero-overlap limit; however, for van der Waals and shorter distances it becomes clouded due to overlap that damps the long-range force laws and due to exchange repulsion, charge transfer, partial or full covalency, and other mean-field and correlation contributions to interaction energies. For example, we evaluated the D3 damped dispersion formula that has been parametrized to add dispersion-like corrections to density functional theory,<sup>17</sup> and we found for the ethylene dimer values of the D3 “dispersion” ranging from 4.2 to 0.1 kcal/mol using various density functionals because this formula not only accounts for damped dispersion but also includes other systematic corrections to available approximate density functionals. The M06-L approximate density functional used here is one of the methods that yields 0.1 kcal/mol, which indicates that its medium-range correlation energy already

**Table 3.** Binding Energies (kcal/mol) and Dispersion Energies (kcal/mol) Calculated Using Grimme's DFT-D3 Method for revPBE38 and HCTH120 Parameters with Zero Damping for the Fe3opt1–guest Systems in the 222 Spin State

guest	$\Delta E^a$	$\Delta E_{\text{disp}}$	$\Delta E_{\text{disp}}$	difference from ethane		
	M06-L	revPBE38	HCTH120	$\Delta \Delta E_{\text{disp}}$	$\Delta \Delta E_{\text{disp}}$	$\Delta \Delta H_{318}^b$
methane	6.7	8.8	7.5	-2.0	-2.8	-1.2
ethane	8.3	10.8	10.3	0.0	0.0	0.0
ethylene	11.9	11.7	12.0	0.9	1.7	4.8
acetylene	12.7	14.0	9.0	3.2	-1.3	5.2
propane	9.8	12.2	10.9	1.4	0.6	1.9
propylene	14.2	16.3	13.9	5.5	3.6	4.5

<sup>a</sup>Positive numbers of  $\Delta E$  or  $\Delta E_{\text{disp}}$  denote attraction (binding). <sup>b</sup>This column is from experiment;<sup>6</sup> the other columns are theoretical. Positive numbers denote more attraction (stronger binding).

includes damped dispersion for the ethylene dimer, so we do not need to add a molecular mechanics term to the present calculations.

To gain insight into the contribution of dispersion-like interactions in binding between the guest molecule and the cluster model, we proceeded as follows. Probably the most successful attempt to sort out the damped dispersion contribution is symmetry-adapted perturbation theory (SAPT),<sup>18</sup> and the damped dispersion contribution to the interaction energy in the ethylene dimer was calculated to be 2.6 kcal/mol by Podeszwa et al.<sup>19</sup> using SAPT. Examining the various dispersion parameter sets of Grimme,<sup>20</sup> we found that the revPBE38<sup>17,20,21</sup> set (with zero damping<sup>17</sup>) gives 2.5 kcal/mol, and therefore we used these parameters to estimate the damped dispersion contributions to the adsorption energies; for comparison we also examined the HCTH120<sup>20–22</sup> parameters which (again with zero damping) give 1.8 kcal/mol. The results for the opt1 geometries for the 88-atom model are in Table 3. It can be seen from this table that  $\Delta E_{\text{disp}}$  calculated by subtracting  $E_{\text{disp}}$  of the cluster–guest complex from that of the separate cluster and the guest molecule, correlates reasonably well with the binding energy,  $\Delta E$ , although neither damped dispersion set correlates with the experimental enthalpies as well as the full M06-L calculations; the damped dispersion sets have mean absolute deviations from experiment of 3.8 and 2.8 kcal/mol, whereas the M06-L energies have mean absolute deviations from the experimental enthalpies of 2.1 kcal/mol. The values for  $\Delta E$  are found to be smaller than  $\Delta E_{\text{disp}}$  (for most of the systems in Table 3), which is not surprising since one must also consider other effects such as exchange repulsion and since the damping of the dispersion in the D3 model is approximate.

In Table 3,  $\Delta \Delta E_{\text{disp}}$  gives, for each hydrocarbon, the difference from ethane of the dispersion contribution to binding, again as evaluated by the D3 term parametrized for revPBE38 or HCTH120. This difference gives us a measure of the extent of dispersion for each hydrocarbon as compared to ethane. This column correlates remarkably well with the  $\Delta \Delta H_{318}$  values for alkanes and alkenes but not for acetylene, which indicates that the interaction energy of acetylene is more complicated.

In another test to check the presence of dispersion-like interactions between the guest molecule and the model cluster, we performed Hartree–Fock (HF) calculations on Fe3opt1 (222 spin state) systems bound to ethane and ethylene. Since the HF method lacks dynamical electron correlation, it does not include dispersion-like interactions between the guest molecule and the cluster model. Table 4 shows a comparison of binding energies at the HF level with those from M06-L calculations. We

**Table 4.** Binding Energies (kcal/mol) Computed at the HF and M06-L Levels Using the def2-TZVP Basis Set for Fe3opt1 Systems (222 Spin State) Bound to Ethane and Ethylene

system	M06-L	HF
Fe3opt1–ethane	8.3	0.9
Fe3opt1–ethylene	11.9	1.5

find that HF results show very small attractive interaction between the guest molecule and the cluster model, which is consistent with most of the attractive interaction energy given by M06-L coming from dispersion-like interactions. Also, the optimized structure at the HF level has the ethane molecule more than 3.9 Å away from the metal center and the ethylene molecule more than 3.3 Å away from the metal center.

**CM5 Charges.** Another important question in understanding the interaction energies is the role of electrostatics. We will consider CM5 charges for two cases in which no gas molecule is bound: (i) the charges on one formula unit of Fe-MOF-74 which is composed of the organic fragment dobdc<sup>4-</sup> and two Fe ions (as estimated from the central part of the cluster models and given in Table 5) and (ii) the charges on the central Fe and the five coordinated oxygens (as given in Table 6). Figure 14a shows the labels on all the atoms of dobdc<sup>4-</sup> and the notation used to represent the oxygen atoms in it. One of the carboxylate oxygen bridges to two neighboring iron centers and is called ca2, and the other carboxylate oxygen bridges only one iron center and is labeled as ca1. The oxido oxygen bridges two iron centers and hence is labeled as ox2. Table 5 gives charges on each atom of one formula unit of Fe<sub>2</sub>(dobdc) as calculated for both the 88-atom and 106-atom models using the Fe3opt0, Fe3opt12, and Fe5opt0 geometries. The spin states considered for each of these geometries are 222 for Fe3opt0 and Fe3opt12 and 22222 for Fe5opt0.

To understand the significance of the charges in Table 5, we made additional calculations on fragments. Figure 14b shows the most stable optimized structure of an isolated 2,5-dioxido-1,4-benzenedicarboxylic acid molecule as obtained by considering various cases of placing two protons on three different types of oxygen atoms (ca1, ca2, and ox2) on one side of the organic linker (Figure 14a) and in exactly the same way on the other side since the organic linker is symmetrical. The CM5 charges of this protonated neutral are compared to the charges in the MOF in Table 5. Calculations on Li<sub>4</sub>(dobdc) were also performed, and its optimum structure was found by replacing the protons of H<sub>4</sub>(dobdc) by Li<sup>+</sup> ions. This is done to see what effect a small electropositive cation, Li<sup>+</sup>, has on the structure and charge of dobdc<sup>4-</sup> in contrast to the transition metal ion, Fe<sup>2+</sup>, and it is

**Table 5. Comparison of M06-L/def2-TZVP/CMS Charges (in Atomic Units) on the Organic Linker Calculated Using an Isolated  $H_4(dobdc)$ , 88-Atom (Fe3opt0), 88-Atom (Fe3opt12), and 106-Atom (Fe5opt0) Models**

	type	atomic number	$H_4(dobdc)$	Fe3opt0	Fe3opt12	Fe5opt0
1		6	-0.09	-0.12	-0.12	-0.11
2		6	0.10	0.12	0.11	0.13
3		6	-0.02	-0.03	-0.03	-0.03
4		6	-0.09	-0.12	-0.12	-0.11
5		6	0.10	0.12	0.11	0.13
6		6	-0.02	-0.03	-0.03	-0.03
7		1	0.12	0.12	0.12	0.12
8		1	0.12	0.12	0.12	0.12
9		6	0.28	0.28	0.29	0.29
10	bridging carboxylate O (ca2)	8	-0.33	-0.33	-0.35	-0.33
11	nonbridging carboxylate O (ca1)	8	-0.37	-0.31	-0.33	-0.33
12		6	0.28	0.28	0.29	0.29
13	bridging carboxylate O (ca2)	8	-0.33	-0.33	-0.35	-0.33
14	nonbridging carboxylate O (ca1)	8	-0.37	-0.31	-0.33	-0.33
15	oxido O (ox2)	8	-0.40	-0.40	-0.40	-0.40
16	oxido O (ox2)	8	-0.40	-0.40	-0.40	-0.40
17	Fe	26		0.67	0.71	0.67
18	Fe	26		0.67	0.71	0.67
	total charge on $Fe_2(dobdc)$			0.00	0.00	0.00

**Table 6. Charges (in Atomic Units) on the Central Iron Ion, the Five Oxygen Atoms in the First Coordination Sphere of the Central Ion, and the Guest Molecule Bound to the Central Iron Ion for the 222 Spin State of the 88-Atom Model Computed Using M06-L/def2-TZVP/CMS**

system	ca1	Fe	guest	ox2	ca2	ox2	ca2
Fe3opt0	-0.35	0.67		-0.40	-0.35	-0.40	-0.32
Fe3opt1	-0.36	0.66		-0.40	-0.35	-0.40	-0.31
Fe3opt12	-0.36	0.71		-0.39	-0.38	-0.40	-0.32
Fe3opt0–ethane	-0.35	0.64	0.04	-0.40	-0.34	-0.40	-0.32
Fe3opt0–ethylene	-0.35	0.63	0.06	-0.40	-0.35	-0.40	-0.32
Fe3opt1–ethane	-0.36	0.64	0.03	-0.40	-0.35	-0.40	-0.31
Fe3opt1–ethylene	-0.36	0.65	0.01	-0.40	-0.33	-0.40	-0.31
Fe3opt12–ethane	-0.36	0.67	0.04	-0.39	-0.38	-0.40	-0.32
Fe3opt12–ethylene	-0.35	0.67	-0.02	-0.39	-0.36	-0.39	-0.31

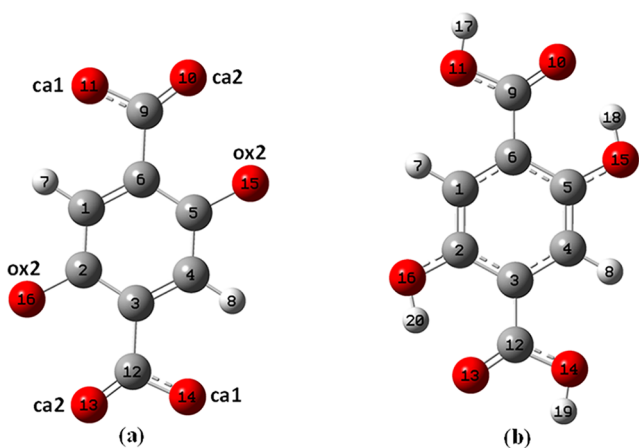


**Figure 14.** (a) Organic linker, 2,5-dioxido-1,4-benzenedicarboxylate ( $dobdc^{4-}$ ), present in Fe-MOF-74, which is the deprotonated form of tetraprotic acid,  $H_4(dobdc)$ , and (b) the isolated tetraprotic acid,  $H_4(dobdc)$ . Three different kinds of oxygen atoms present in the organic linker denoted by ca1, ca2, and ox2. [Color code: red = oxygen, gray = carbon, white = hydrogen].

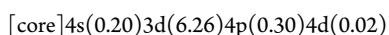
found that even the  $Li^+$  cation causes less distortion of the structure of the benzene ring than is seen in the experimental

structure. A detailed comparison of geometries and CMS charges of  $H_4(dobdc)$ ,  $Li_4(dobdc)$ , and  $Fe_2(dobdc)$  from the experimental structure is presented in the Supporting Information, but the key lesson drawn from Table 5 is that, despite the large distortions in the experimental structure (which may need further refinement), the qualitative nature of the charge distribution in the organic linker is not greatly perturbed from that in the neutral molecule, although the charge differences between the corresponding atoms when we compare  $H_4(dobdc)$  with Fe3opt0 show a significant maximum difference of 0.06 units of charge. Table 5 shows that the variation in charge for each atom is less pronounced when we increase the cluster size by going from Fe3opt0 to Fe5opt0, with the maximum difference for the two models being 0.02 units of charge. Optimization of 12 atoms of the 88-atom model increases the charge on the iron ion from 0.67 atomic units in Fe3opt0 to 0.71 atomic units in Fe3opt12 (which is correlated to the iron ions coming closer in Fe3opt12 as compared to Fe3opt0). The differences in CMS charges are within 0.02 units of charge when we compare Fe3opt0 and Fe3opt12 for the rest of the atoms (C, O, and H) in Table 5.

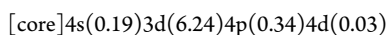
Table 6 shows the charges on the central iron ion and the five oxygen atoms surrounding it in the bare MOF and the MOF bound to ethane and ethylene and the total charges on the bound

guest molecules, ethane and ethylene. These two molecules have been chosen to see how the partial atomic charges and the orbital energies of the iron ion change upon going from a bare MOF with a distorted square pyramidal structure to the MOF bound to a guest molecule, where the structure is a distorted octahedron. The charges reported in Table 6 are for all three levels of optimization of the 88-atom model. If we consider the case for Fe3opt0, we see that the charge on the central iron ion decreases from 0.67 to 0.64 and 0.63 on binding to ethane and ethylene, respectively, which is due to a small amount of charge transfer from these guest molecules to the metal center. The total charges (obtained by summing up the charges of all the atoms of the guest molecule) remaining on ethane and ethylene are 0.04 and 0.06 atomic units, respectively. This implies that ethylene donates slightly more negative charge to the central iron ion than ethane and makes it less positive. For Fe3opt1, we observe that ethane has a more positive charge (0.03 atomic units) than ethylene (0.01 atomic units) and makes the central iron less positive (0.64 atomic units) compared to the bare Fe3opt1 (0.66 atomic units). The charge on the iron center for Fe3opt12 decreases from 0.71 to 0.67 on binding to both ethane and ethylene; this indicates that some charge transfer from ethane and ethylene occurs to the metal center. If we look at the total charge on these guest molecules bound to the metal center, it can be seen that the charge on ethane is 0.04 atomic units and on ethylene is -0.02 atomic units. Positive charge on ethane implies that a small amount of charge transfer from ethane to the metal center occurs, but a negative charge on ethylene implies a possibility of back-donation of electrons from the filled d orbitals of the central iron ion to the vacant orbitals on ethylene. We also observe from Table 6 that the total charge on ethylene decreases from 0.06 to 0.01 to -0.02 with an increasing level of optimization from Fe3opt0 to Fe3opt12, while that on ethane shows much less variation, which could imply that back-donation of electrons from the metal center to ethylene increases with an increase in the level of optimization. A more detailed table (Table S6) in the Supporting Information on the charges of each atom of the guest molecule shows that the carbon atoms of ethylene become more negative with increasing level of optimization which could again indicate the possibility of back-donation. To test this property, natural bond orbital (NBO) analysis<sup>23</sup> has been performed for all three levels of optimization (vide infra), and this will be considered next.

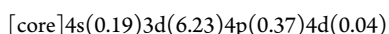
**NBO Analysis.** NBO analysis has been performed for three species (bare MOF, MOF bound to ethane, and MOF bound to ethylene) to gain insights into the bonding between the guest molecule and the central iron ion in the 88-atom model. Although absolute magnitudes of the partial atomic charges from NBO analysis do not agree with our best estimates, this analysis provides a physical interpretation of the nature of the bonding. Our analysis with Fe3opt0 geometries shows that when the guest is bound to the open site of the iron ion in the MOF the natural electron configuration of the central iron ion is changed from



for bare MOF to



for MOF bound to ethane and to



for MOF bound to ethylene. These populations show the presence of weak electron donation from the  $\pi$  bonding orbital of

ethylene and  $\sigma$  bonding orbital of the C–H bond of ethane to the 3d, 4p, and 4d orbitals of the central Fe ion. The NBO analysis using the Fe3opt1 geometries, where the central iron ion of the cluster is optimized, shows not only much stronger electron donation from ethylene to the central iron ion but also notable electron back-donation from the 3d orbitals of the central iron ion to the  $\pi$  antibonding orbital of ethylene. This agrees well with CMS charge analysis as shown in Table 6; when Fe3opt1–ethylene geometry is used, the net charge located in ethylene is only 0.01, much smaller than 0.06 observed using the Fe3opt0–ethylene geometry. The NBO analysis with the Fe3opt1 geometry indicates that the stronger binding energy of ethylene with MOF compared to ethane is also a result of the  $\pi$  bond interaction between ethylene and iron besides stronger dispersion interaction. The Fe3opt12–C<sub>2</sub>H<sub>4</sub> geometry has a shorter Fe–C bond distance, and the NBO analysis shows an Fe–C single bond, which is not observed for Fe3opt0–C<sub>2</sub>H<sub>4</sub> and Fe3opt1–C<sub>2</sub>H<sub>4</sub>. This explains the larger binding enthalpies calculated with Fe3opt12 geometries than those calculated with Fe3opt0 and Fe3opt1 geometries for MOF bound to ethylene. The NBO analysis with Fe3opt1–ethane and Fe3opt12–ethane geometries does not show stronger electron donation from ethane to the iron ion than with Fe3opt0–ethane nor any electron back-donation.

**Orbital Energy Analysis.** Figure 15 shows the natural atomic orbital<sup>23</sup> (NAO) energy level splitting of the five

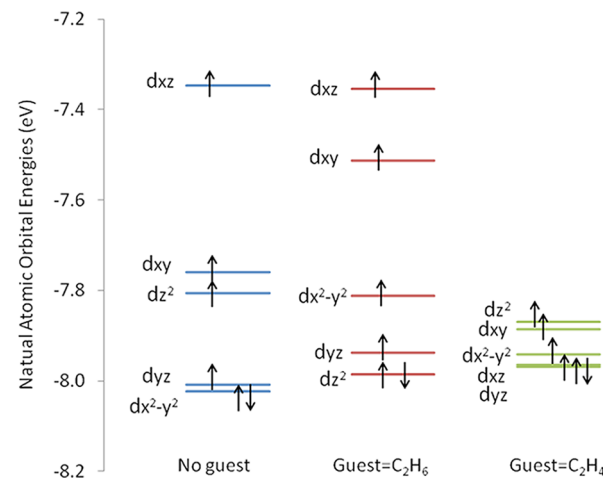


**Figure 15.** Splitting of the d orbitals of the central iron ion of the 88-atom model with Fe3opt1 geometries in the absence and presence of the guest molecules, ethane and ethylene. The energy levels shown in the figure are the NAO energies of the  $\alpha$  spin orbitals, although we show both  $\alpha$  and  $\beta$  spin orbital occupancies. (The  $\beta$  spin orbitals, most of which are unoccupied, have different energies in the unrestricted open-shell treatment employed here; however, showing them would complicate the plot too much, and the energies for the majority  $\alpha$  spin are more relevant.)

degenerate d-orbitals of the Fe<sup>2+</sup> cation obtained from NBO analysis in two ligand fields: one is in a distorted square pyramidal environment of the five oxygen atoms surrounding the central iron ion, and the other one is in a distorted octahedral environment created by the presence of a guest molecule along with five oxygen atoms. The Fe3opt1 geometries of the 88-atom model bound to guest are used instead of Fe3opt12 geometries here because based on our binding enthalpy calculations and NBO analysis the Fe3opt12 could overestimate the interaction between MOF and ethylene. We can see from Figure 15 that in

the absence of a guest molecule the central iron ion of the 88-atom model shows the expected splitting<sup>12</sup> of d orbitals for a distorted square pyramidal environment around a metal center. The presence of ethane or ethylene in the vacant site of the central iron ion makes the environment around it a distorted octahedron, and the splitting of d orbitals occurs as expected<sup>12</sup> with three of the five d orbital energies getting closer to one another and having lower energy than the other two. The stronger interaction of ethylene with the MOF causes a remarkable change in the orbital energy levels of the d orbitals of the Fe ion, as compared to ethane. The splitting of the d orbitals of the MOF bound to ethylene is more similar to the splitting of d orbitals in an octahedral ligand field.

## 5. CONCLUSIONS

An 88-atom model and a 106-atom model of a well-known metal–organic framework, Fe-MOF-74, have been introduced based on its experimental crystal structure. These two models are used to investigate the properties of Fe-MOF-74 and its binding abilities to C1–C3 hydrocarbons by density functional theory with the M06-L density functional. The four high-spin states ( $2\bar{2}2$ ,  $2\bar{2}\bar{2}$ ,  $\bar{2}\bar{2}\bar{2}$ , and  $\bar{2}\bar{2}\bar{2}$ ) of the 88-atom model with three irons and one spin state  $2\bar{2}2\bar{2}2$  of the 106-atom model with five irons, in which each iron is in a local quintet state, have been considered.

The present study shows that the magnitude of binding enthalpies for unsaturated hydrocarbons is higher than those for saturated hydrocarbons. This agrees with the experimental results. These binding enthalpies for a given hydrocarbon have similar values for the four cases of spin states of the 88-atom model considered in this study. NBO analysis shows that there exists weak electron donation from  $\pi$ -bonding orbital of ethylene and  $\sigma$ -bonding orbital of the C–H bond of ethane to the 3d, 4p, and 4d orbitals of the central Fe ion. The filled d-orbitals on the d<sup>6</sup> metal center can share electrons with unsaturated hydrocarbons and hence contribute to stronger binding. However, the bonding trends in all cases except acetylene also correlate with differences in estimates of the damped dispersion contribution, which is included implicitly in the M06-L density functional. The computed values of CMS charges indicate that the charge on the metal center and the five oxygen atoms in its coordination sphere do not vary much upon optimization.

## ■ ASSOCIATED CONTENT

### Supporting Information

The binding energies and enthalpies for all spin states at all levels of optimization, the coordinates and the absolute energies in hartrees of selected structures, and further details of the analysis of damped dispersion, CMS charges, and geometries. This material is available free of charge via the Internet at <http://pubs.acs.org>.

## ■ AUTHOR INFORMATION

### Corresponding Author

\*E-mail: truhlar@umn.edu.

### Notes

The authors declare no competing financial interest.

## ■ ACKNOWLEDGMENTS

The authors are grateful to Allison Dzubak, Laura Gagliardi, Jeff Long, Andy Luo, Wendy Queen, and Bo Wang for helpful assistance or discussions. The research was supported by the U.S.

Department of Energy, Office of Basic Energy Sciences, Division of Chemical Sciences, Geosciences and Biosciences under Award DE-FG02-12ER16362 to the Nanoporous Materials Genome Center.

## ■ REFERENCES

- (1) Furukawa, H.; Ko, N.; Go, Y. B.; Aratani, N.; Choi, S. B.; Choi, E.; Yazaydin, A. O.; Snurr, R. Q.; O'Keeffe, M.; Kim, J.; et al. Ultrahigh Porosity in Metal–Organic Frameworks. *Science* **2010**, *329*, 424–428.
- (2) (a) Rowsell, J. L. C.; Yaghi, O. M. Strategies for Hydrogen Storage in Metal–Organic Frameworks. *Angew. Chem., Int. Ed.* **2005**, *44*, 4670–4679. (b) Dincă, M.; Long, J. R. Hydrogen Storage in Microporous Metal–Organic Frameworks with Exposed Metal Sites. *Angew. Chem., Int. Ed.* **2008**, *47*, 6766–6779. (c) Furukawa, H.; Yaghi, O. M. Storage of Hydrogen, Methane, and Carbon Dioxide in Highly Porous Covalent Organic Frameworks for Clean Energy Applications. *J. Am. Chem. Soc.* **2009**, *131*, 8875–8883. (d) Murray, L. J.; Dincă, M.; Long, J. R. Hydrogen Storage in Metal–Organic Frameworks. *Chem. Soc. Rev.* **2009**, *38*, 1294–1314. (e) Sumida, K.; Hill, M. R.; Horike, S.; Dailly, A.; Long, J. R. Synthesis and Hydrogen Storage Properties of Be<sub>12</sub>(OH)<sub>12</sub>(1,3,5-benzenetribenzoate)<sub>4</sub>. *J. Am. Chem. Soc.* **2009**, *131*, 15120–15121.
- (3) (a) Fujita, M.; Kwon, Y. J.; Washizu, S.; Ogura, K. Preparation, Clathration Ability, and Catalysis of a Two-Dimensional Square Network Material Composed of Cadmium(II) and 4,4'-Bipyridine. *J. Am. Chem. Soc.* **1994**, *116*, 1151–1152. (b) Ma, L.; Lin, W. Chirality-Controlled and Solvent-Templated Catenation Isomerism in Metal–Organic Frameworks. *J. Am. Chem. Soc.* **2008**, *130*, 13834–13835. (c) Ma, L.; Abney, C.; Lin, W. Enantioselective Catalysis with Homochiral Metal–Organic Frameworks. *Chem. Soc. Rev.* **2009**, *38*, 1248–1256.
- (4) McDonald, T. M.; Lee, W. R.; Mason, J. A.; Wiers, B. M.; Hong, C. S.; Long, J. R. Capture of Carbon Dioxide from Air and Flue Gas in the Alkylamine-Appended Metal–Organic Framework mmen-Mg<sub>2</sub>(dobpdc). *J. Am. Chem. Soc.* **2012**, *134*, 7056–7065.
- (5) Bloch, E. D.; Murray, L. J.; Queen, W. L.; Chavan, S.; Maximoff, S. N.; Bigi, J. P.; Krishna, R.; Peterson, V. K.; Grandjean, F.; Long, G. J.; et al. Selective Binding of O<sub>2</sub> over N<sub>2</sub> in a Redox-Active Metal–Organic Framework with Open Iron(II) Coordination Sites. *J. Am. Chem. Soc.* **2011**, *133*, 14814–14822.
- (6) Bloch, E. D.; Queen, W. L.; Krishna, R.; Zadrozny, J. M.; Brown, C. M.; Long, J. R. Hydrocarbon Separations in a Metal–Organic Framework with Open Iron(II) Coordination Sites. *Science* **2012**, *335*, 1606–1610.
- (7) Zhao, Y.; Truhlar, D. G. A New Local Density Functional for Main-Group Thermochemistry, Transition Metal Bonding, Thermochemical Kinetics, and Noncovalent Interactions. *J. Chem. Phys.* **2006**, *125*, 194101/1–18.
- (8) Zhao, Y.; Truhlar, D. G. Density Functionals with Broad Applicability in Chemistry. *Acc. Chem. Res.* **2008**, *41*, 157–167.
- (9) Frisch, M. J.; Trucks, G. W.; Schlegel, H. B.; Scuseria, G. E.; Robb, M. A.; Cheeseman, J. R.; Scalmani, G.; Barone, V.; Mennucci, B.; Petersson, G. A.; et al. *Gaussian 09*, Revision C.01; Gaussian, Inc.: Wallingford, CT, 2010.
- (10) Weigend, F.; Ahlrichs, R. Balanced Basis Sets of Split Valence, Triple Zeta Valence and Quadruple Zeta Valence Quality for H to Rn: Design and Assessment of Accuracy. *Phys. Chem. Chem. Phys.* **2005**, *7*, 3297–3305.
- (11) Zhou, W.; Wu, H.; Yildirim, T. Enhanced H<sub>2</sub> Adsorption in Isostructural Metal–Organic Frameworks with Open Metal Sites: Strong Dependence of the Binding Strength on Metal Ions. *J. Am. Chem. Soc.* **2008**, *130*, 15268–15269.
- (12) Yamamoto, A. *Organotransition Metal Chemistry*; Wiley: New York, 1986.
- (13) Marenich, A. V.; Cramer, C. J.; Truhlar, D. G. *CMS-PAC*; University of Minnesota: Minneapolis, 2011.
- (14) Hirshfeld, F. L. Bonded-Atom Fragments for Describing Molecular Charge Densities. *Theor. Chim. Acta* **1977**, *44*, 129–138.

- (15) Marenich, A. V.; Jerome, S. V.; Cramer, C. J.; Truhlar, D. G. Charge Model 5: An Extension of Hirshfeld Population Analysis for the Accurate Description of Molecular Interactions in Gaseous and Condensed Phases. *J. Chem. Theory Comput.* **2012**, *8*, 527–541.
- (16) Mantina, M.; Valero, R.; Cramer, C. J.; Truhlar, D. G. In *CRC Handbook of Chemistry and Physics*, 93<sup>rd</sup> ed.; Lide, D. R., Ed.; CRC Press: Boca Raton, FL, 2012; Chapter 9, p 49.
- (17) Grimme, S.; Antony, J.; Ehrlich, S.; Krieg, H. A Consistent and Accurate Ab Initio Parametrization of Density Functional Dispersion Correction (DFT-D) for the 94 Elements H–Pu. *J. Chem. Phys.* **2010**, *132*, 154104/1–19.
- (18) Jeziorski, B.; Moszynski, R.; Szalewicz, K. Perturbation Theory Approach to Intermolecular Potential Energy Surfaces of van der Waals Complexes. *Chem. Rev.* **1994**, *94*, 1887–1930.
- (19) Podeszwa, R.; Pernal, K.; Patkowski, K.; Szalewicz, K. Extension of the Hartree–Fock Plus Dispersion Method by First-Order Correlation Effects. *J. Phys. Chem. Lett.* **2010**, *1*, 550–555.
- (20) The parameters of the D3 damped dispersion terms are available at <http://www.thch.uni-bonn.de/tc/downloads/DFT-D3/functionals.html>.
- (21) Goerigk, L.; Grimme, S. A Thorough Benchmark of Density Functional Methods for General Main Group Thermochemistry, Kinetics, and Noncovalent Interactions. *Phys. Chem. Chem. Phys.* **2011**, *13*, 6670–6688.
- (22) Boese, A. D.; Doltsinis, N. L.; Handy, N. C.; Sprik, M. New Generalized Gradient Approximation Functionals. *J. Chem. Phys.* **2000**, *112*, 1670–1678.
- (23) (a) Foster, J. P.; Weinhold, F. Natural Hybrid Orbitals. *J. Am. Chem. Soc.* **1980**, *102*, 7211–7218. (b) Reed, A. E.; Weinhold, F. Natural Bond Orbital Analysis of Near-Hartree–Fock Water Dimer. *J. Chem. Phys.* **1983**, *78*, 4066–4073. (c) Reed, A. E.; Weinstock, R. B.; Weinhold, F. Natural-Population Analysis. *J. Chem. Phys.* **1985**, *83*, 735–746. (d) Reed, A. E.; Weinhold, F. Natural Localized Molecular Orbitals. *J. Chem. Phys.* **1985**, *83*, 1736–1740. (e) Carpenter, J. E. Extension of Lewis Structure Concepts to Open-Shell and Excited-State Molecular Species. *Ph.D. Thesis*, University of Wisconsin, Madison, WI, 1987. (f) Carpenter, J. E.; Weinhold, F. Analysis of the Geometry of the Hydroxymethyl Radical by the Different Hybrids for Different Spins Natural Bond Orbital Procedure. *J. Mol. Struct. (THEOCHEM)* **1988**, *46*, 41. (g) Reed, A. E.; Curtiss, L. A.; Weinhold, F. Intermolecular Interactions from a Natural Bond Orbital, Donor–Acceptor Viewpoint. *Chem. Rev.* **1988**, *88*, 899. (h) Weinhold, F.; Carpenter, J. E. In *The Structure of Small Molecules and Ions*, 1st ed.; Naaman, R.; Vager, Z., Ed.; Springer: New York, 1988; p 227.